ACS OMEGA

Open Access

http://pubs.acs.org/journal/acsodf

Article

Rutin-Loaded Transethosomal Gel for Topical Application: A Comprehensive Analysis of Skin Permeation and Antimicrobial Efficacy

Mohammed F. Aldawsari, Aftab Alam, and Mohd Imran*

Cite This: *ACS Omega* 2024, 9, 27300−27311

Read Online

ACCESS | Metrics & More | Article Recommendations

ABSTRACT: This study conducts a systematic investigation of the creation and optimization of a rutin-loaded transethosome intended for topical use. The formulation's characteristics were thoroughly assessed for vesicle size (160.45 ± 1.98 nm), polydispersity index (0.235 ± 0.067), and zeta potential (−22.89 mV), with an entrapment efficiency and drug loading of 89.99 ± 1.55% and 8.9 ± 2.11%, respectively, and found to have a spherical shape by the use of transmission electron microscopy. The conversion to a gel suitable for application on the skin was carried out. The drug release form Opt-RUT-TE formulation (73.61 ± 2.55%) was significantly higher than that of release form RUT-suspension (34.52 ± 1.19%). The drug that permeated the skin from Opt-RUT-TEG (935.25 ± 10.49 $\mu g/cm^2$) was significantly higher than the permeability from RUT-Suspension gel (522.57 ± 6.79 $\mu g/cm^2$). Notably, tape stripping analysis revealed that the Opt-RUT-TE gel effectively penetrated the skin layers, with a higher concentration observed in the epidermis-dermis than in the RUT-suspension gel. The transethosomal gel exhibited favorable characteristics, highlighting its capacity to efficiently permeate the skin and suppress the growth of microorganisms, and Opt-RUT-TEG showed a higher microorganism inhibition zone (Gram-positive bacteria) than that of RUT-suspension gel. The investigation highlights the significant therapeutic possibilities of rutin in a transethosomal gel formulation for treating dermatological diseases by improving skin permeability and exhibiting antibacterial effects.

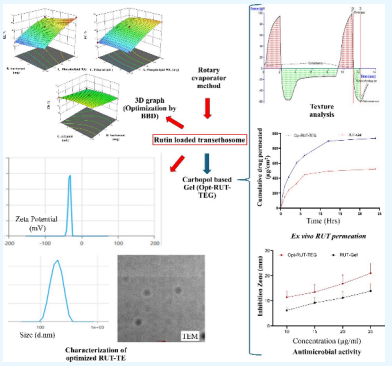

1. INTRODUCTION

Dermatological conditions are prevalent and significantly affect the quality of life of sufferers.[1] Above, there is a list of more than 1000 diseases that affect the skin or are related to the skin. These diseases are categorized into 10 different groups based on the International Classification of Disease.[2] Bacterial skin infections are a significant global healthcare concern, often resulting in frequent emergency treatment.[3] These infections are commonly caused by disease-causing bacteria that invade both outer layers of the skin. They can be classified as either superficially localized or deeper skin infections.[4] Historically, *Staphylococcus aureus*, a bacterium that naturally resides on the skin of around 30% of individuals, has been recognized as the primary reason for skin infections.[5]

Rutin (3′,4′,5,7-tertrahyrdroxy-flavone-3-rutinoside), also referred to as quercetin-3-rutinoside or sophorin, is a compound consisting of the flavonol quercetin and the disaccharide rutinose.[6] Rutin exhibits notable antioxidant capabilities against several oxidizing species, such as hydroxyl, superoxide, and peroxyl radicals.[7] Hence, it harnesses various pharmacological functions including antiallergic,[8] antiaging,[9] anti-inflammatory,[10] anticancer,[11] antibacterial,[12] antiviral,[13] vasoactive, and antiprotozoal effects.[14] Over 70 plant species, such as *Ruta graveolens* L. (Rutaceae) and *Sophora japonica* L. (Fabaceae), have been proven to be excellent sources of rutin. Other examples include *Strelitzia reginae Banks ex Aiton* (Strelitziaceae), *Maranta leuconeura* (Marantaceae), *Orchidantha maxillarioides* (Lowiaceae), *Eucalyptus* spp. (Myrtaceae), *Canna indica* L. (Cannaceae), and *Canna edulis Ker Gawl* (Cannaceae).[15] The antibacterial properties of these plant species have been attributed to flavonoids, terpenoids, and tannins.[16] Flavonoids are typically found in cells that undergo photosynthesis.[17] Moreover, rutin, a compound found in various plant species, demonstrates diverse pharmacological effects including potent antioxidant activity against reactive oxygen species. Notably, studies have established rutin's effectiveness against both Gram-positive and Gram-negative bacterial strains, underscoring its potential for combating antibiotic resistance.[18] Throughout history, formulations containing these substances have been employed to alleviate human ailments. The antibacterial potentials of this class of

Received: February 22, 2024
Revised: May 28, 2024
Accepted: May 30, 2024
Published: June 10, 2024

Table 1. Independent Factors Used to Optimize Transethosomal Preparations and the Resulting Outcomes of Dependent Variables

	A	B	C	Y_1	Y_2
Formulations run	Phospholipid 90G (mg)	Sodium cholate (mg)	Ethanol (mL)	EE (%)	Drug permeation ($\mu g/cm^2$)
1	120	30	11	72.44	814.94
2	140	20	11	80.99	935.25
3	140	10	7	83.98	899.49
4	140	20	11	81.01	934.84
5	160	10	11	88.99	965.98
6	140	30	15	78.98	887.94
7	140	20	11	81.47	932.89
8	120	10	11	75.89	819.98
9	140	10	15	82.41	929.45
10	160	20	15	82.49	961.55
11	140	30	7	79.49	914.55
12	120	20	7	75.11	811.49
13	140	20	11	82.99	935.25
14	140	20	11	81.37	933.24
15	160	20	7	86.04	955.49
16	120	20	15	73.11	816.97
17	160	30	11	84.19	951.98

natural compounds have made them the primary focus of investigation.[19] Rutin is primarily hindered by its reduced bioavailability, which is mostly due to its low solubility in water, instability, and restricted capacity to pass through cell membranes.[20]

For active substances to reach their target site and work therapeutically, they must overcome the stratum corneum (SC), a rate-limiting skin barrier. Although the SC protects against infections and xenobiotics, it can also impede drug penetration and hinder the transit of active components.[21] Current research encapsulates rutin in nanocarriers for skin delivery to address this constraint.[22] Nanocarriers improve skin permeability, active component retention, drug release, hydrophilic and lipophilic drug incorporation, and the target effect. Ethosomes are a unique carrier with improved skin delivery due to their great deformability and flexibility. Ethosomes, like liposomes, have a phospholipid bilayer and are biocompatible but have a higher ethanol concentration. Depending on composition, ethanol gives ethosomes specific features such as nanovesicular size, great deformability, fluidity, and stability.[23] Transethosomes (TEs) are an upgrade of ethosomes, containing an edge activator and ethanol, possessing the ability to penetrate the skin more deeply and provide protection against skin infections. This makes them well suited for delivering substances directly to specific areas of the skin.[24] Transethosomes are formed by combining ethanol and an edge activator, resulting in a combination of the advantages offered by ethosomes and deformable liposomes. As TEs, they can change shape to reach the innermost skin layers without harm. Ethanol and sodium cholate in TE help stratum corneum-trapped drugs migrate.

Furthermore, transethosomes improved deposition and penetration.[25] Carbomers are synthetic polymers derived from poly(acrylic acid) with a high molecular weight. They are cross-linked with either allyl sucrose or allyl pentaerythritol. These substances have anionic character and consist of 56 to 68% w/w carboxylic acid groups.[26] Viscosity regulates the process of drug being absorbed into the body and the duration it remains on the skin. The carboxy vinyl polymer (Carbopol 934) was used as a gelling agent, and it is advantageous in topical gels since it exhibits minimal changes in viscosity within the pH range of 5−8.[27]

The development of a rutin-based topical antimicrobial formulation presents a justified advancement over existing treatments due to rutin's established efficacy against both Gram-positive and Gram-negative bacteria, which is critical in combating antibiotic resistance. Furthermore, the utilization of innovative nanoformulations such as nanostructured lipid carriers, ethosomes, and glycerosomes enables the incorporation of rutin for sun protection, antioxidant efficacy, and antibacterial properties, promising superior therapeutic outcomes compared to conventional treatments.[18,28,29] This integration of rutin into advanced nanoformulations not only enhances its efficacy but also expands its potential applications, addressing multiple aspects of skin health and offering a comprehensive approach to dermatological care.

The present study methodically developed and optimized a transethosome formulation loaded with rutin employing the rotary evaporator method and the Box-Behnken design (BBD) methodology, respectively. The resulting formulation was then analyzed for vesicle size, polydispersity index, zeta potential, and transmission electron microscopy. Additionally, the formulation was transformed into a gel for topical administration. The formulated gel was examined for its efficacy against Gram-positive bacteria and *in vitro* drug release and its effectiveness in *ex vivo* drug permeation and tape stripping studies to assess its ability to penetrate the skin. These investigations offer a comprehensive strategy to improve the therapeutic potential of rutin in topical applications for skin-related ailments.

2. RESULTS AND DISCUSSION

2.1. Optimization of RUT-TE. A total of 17 runs were obtained, with 5 of them being center points, while the remaining 12 runs were within the limit of error. The comprehensive analysis of each of the 17 batches is presented in Table 1. The statistical significance of the model was assessed using ANOVA. The quadratic model was determined to be the most appropriate for all of the responses. For each

https://doi.org/10.1021/acsomega.4c01718
ACS Omega 2024, 9, 27300−27311

Table 2. Statistical Parameters by ANOVA

Responses (Y_1, Y_2)	Model	R^2	Adjusted R^2	Predicted R^2	SD	CV %	F value
Entrapment efficiency %	Quadratic	0.9785	0.9509	0.7802	0.9864	1.22	2.01
Drug permeation $\mu g/cm^2$	Quadratic	0.9995	0.9989	0.9936	1.86	0.205	4.89

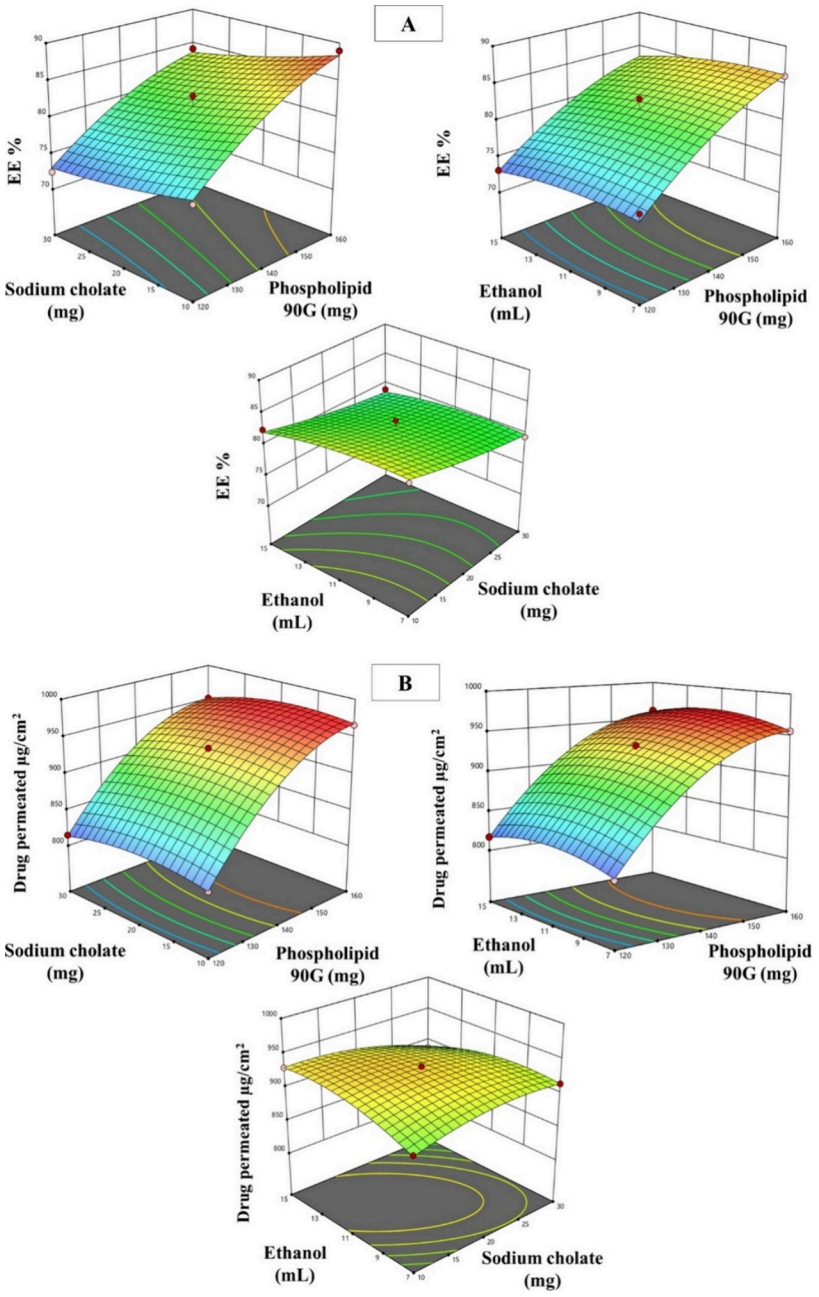

Figure 1. (A and B) 3D graph depicting the effect of independent variables (Phospholipid 90G, edge activator, and ethanol) on the dependent variable entrapment efficiency % (Y_1) and drug permeability $\mu g/cm^2$ (Y_2).

dependent variable, Table 2 provides the R^2, CV %, SD, and F values.

2.1.1. Effect of Independent Variables on Entrapment Efficiency % (Y_1). The entrapment efficiencies varied between a minimum value of 72.44% and a high value of 88.99%, as indicated in Table 1. The polynomial equation below demonstrated that the concentration of phospholipids (A, mg) had a synergistic effect on the drug EE, whereas the concentrations of surfactant (B, mg) and ethanol (C, mL) had a detrimental effect.

$$EE\% = +81.57 + 5.65A - 2.02B - 0.9538C - 0.3875AC + 0.2650BC - 1.61A^2 + 0.4195B^2 - 0.775C^2$$

The increase in encapsulation efficiency with higher phospholipid content can be related to the drug's lipophilicity, as lipophilic drugs tend to be enclosed within the phospholipid phase of the vesicles[30] as can be seen in Figure 1A. Another contributing factor to the enhancement of entrapment efficiency could be the increase in lipid content, which

https://doi.org/10.1021/acsomega.4c01718
ACS Omega 2024, 9, 27300−27311

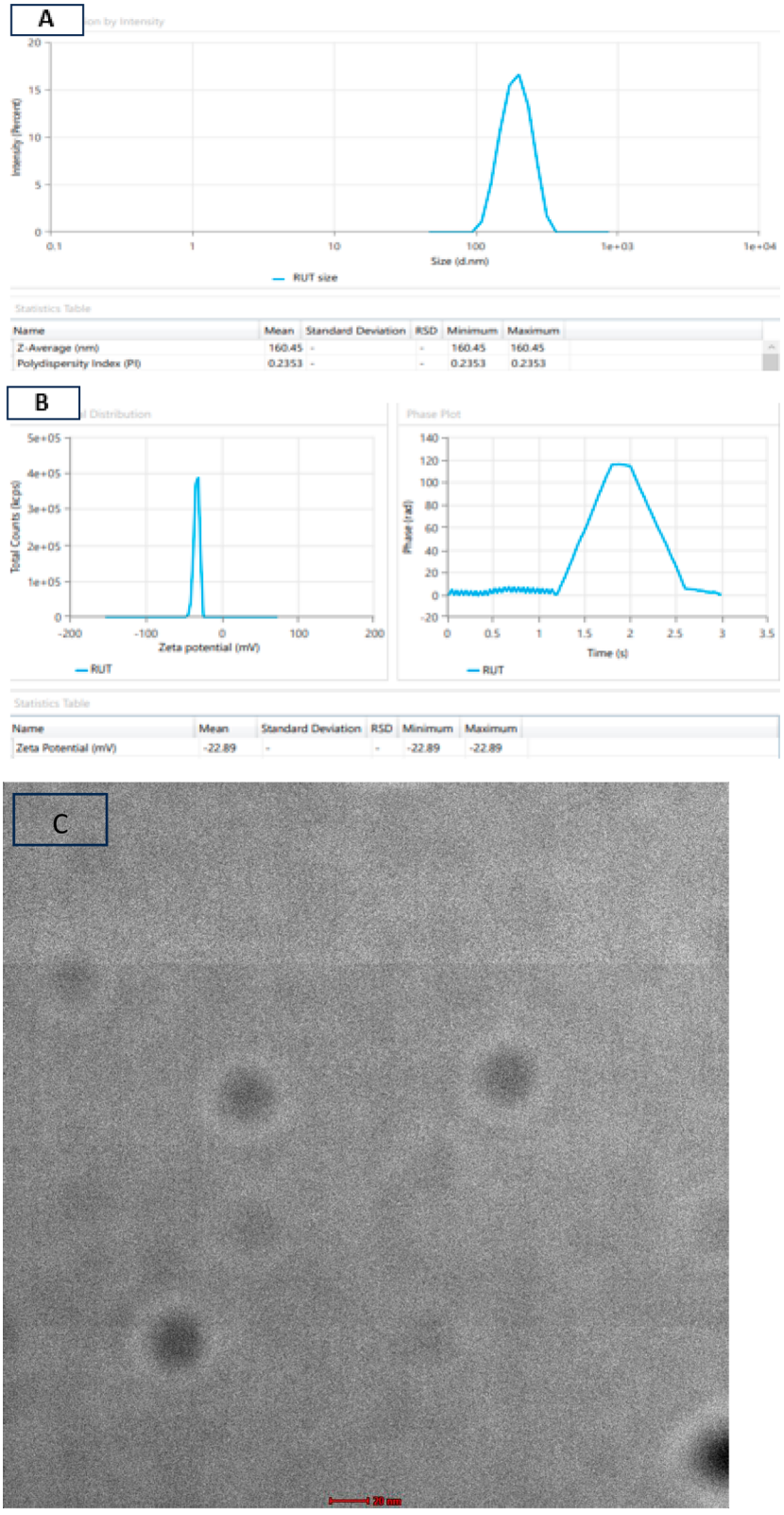

Figure 2. (A) Vesicle size, (B) zeta potential, and (C) TEM image of Opt-RUT-TE.

provides additional space for encapsulating drug molecules within the vesicles. Additionally, it decreases the diffusion of the drug into the surrounding aqueous phase, resulting in an improvement in encapsulation efficiency.[31] The findings from Figure 1A and Table 1 clearly illustrate that the presence of a surfactant has a detrimental effect on the entrapment efficiency. With an increase in surfactant concentration, there is a corresponding drop in entrapment efficiency. The existence of pores inside the bilayers of the vesicles results in the liberation of the encapsulated drug as a consequence of leakage.[32] Moreover, an increased concentration of surfactant facilitated the production of mixed micelles, which coexisted

https://doi.org/10.1021/acsomega.4c01718
ACS Omega 2024, 9, 27300−27311

with the transethosomal vesicles in the formulations.[33,34] Similarly, the entrapment effectiveness of the ethosomal formulation increases as the ethanol concentration increases from 7 to 11 mL, but beyond that, the entrapment decreases as the concentration of ethanol increases. This is due to the increased fluidity of the membrane and the increased permeability of the vesicles, resulting in a decrease in entrapment efficiency. The higher ethanol concentration in ethosomes likely enhanced the flexibility of the vesicle membrane by lowering the interfacial tension.[35]

2.1.2. Effect of Independent Variables on Drug Permeation. The drug permeation varied between a minimum value of 811.49 $\mu g/cm^2$ and a high value of 965.98 $\mu g/cm^2$, as indicated in Table 1. The polynomial equation below demonstrated that the concentration of phospholipids (A, mg) and ethanol (C, mL) had a synergistic effect on the drug permeation, whereas the concentrations of surfactant (B, mg) had a detrimental effect as shown in Figure 1B.

$$\text{Drug permeation } \mu g/cm^2 = +934.29 + 71.45A - 5.69B + 1.86C - 2.24AB + 0.1450AC - 14.14BC - 33.78A^2 - 12.30B^2 - 14.14C^2$$

The increase in drug permeation with the increase in phospholipid concentration could be due to their occlusive effect on the skin leading to increased skin moisture and flexibility, which promotes the absorption of drugs. This effect is achieved through the interaction of the physiological lipid composition with the stratum corneum, which affects the reorganization of its lipids and improves the penetration of molecules.[36] Similarly, an increase in ethanol concentration leads to an increase in drug permeability, a phenomenon often attributed to the ethanol effect. This effect occurs as ethanol interacts with the lipid molecules in the polar headgroup region, altering the lipid bilayer's structure and enhancing permeability. This interaction leads to a decrease in the transition temperature of lipids in the stratum corneum, resulting in increased fluidity and decreased density of the lipid multilayer.[37] By introducing ethanol, the vesicles acquired flexible properties, enabling the ethosomal vesicles to penetrate more easily and deeply into the underlying layers of the skin.[38] In contrast, an increase in surfactant concentration from 10 to 20 mg leads to an increase in drug permeability. This can be attributed to the surfactant modifying the permeability of the membrane. However, when the surfactant concentration is further increased from 20 to 30 mg, it results in reduced drug permeation. This could be due to the drug molecules being trapped within the micelles and becoming unavailable for permeation.[39,40]

2.2. Optimized Batch. An evaluation was performed to verify the experimental design of the optimized formulation. The findings revealed that the optimal composition comprises 157.94 mg of phospholipid 90G, 10.65 mg of sodium cholate, and 10.31 mL of ethanol. The experimental results exhibited a high degree of similarity, hence confirming the validity and dependability of the optimized formulation.

2.3. Characterization of Opt-Rut-TE. *2.3.1. Determination of Vesicle Size, PDI, Zeta Potential, and TEM.* The vesicle size and PDI of the Opt-RUT-TE were found to be 160.45 ± 1.98 nm and 0.235 ± 0.067, respectively (Figure 2A). A wider spread of particles is indicated by lower values of the polydispersity index. The zeta potential value of Opt-RUT-TE was found to be −22.89 mV as shown in Figure 2B. The observed zeta potential values suggest that the dispersions maintain their deflocculated state due to the presence of electrostatic repulsion among the particles. This electrostatic repulsion contributes to the physical stability of the dispersions over a period of time.[41] The TEM image revealed that the vesicles produced by Opt-RUT-TE were spherical in shape as shown in Figure 2C.

2.3.2. Entrapment Efficiency and Drug Loading. The entrapment efficiency and drug loading of the Opt-RUT-TE formulation were found to be 83.98 ± 2.49% and 8.39 ± 1.74%, respectively. The enhancement of hydrophobic drug solubilization can be achieved through the utilization of edge activators in transethosomal formulations. This leads to an improvement in the drug entrapment efficiency and drug loading of the formulations.[42]

2.4. *In Vitro* Drug Release. In comparison to the release of RUT from formulation Opt-RUT-TE (73.61 ± 2.55%), the release of RUT *in vitro* from a RUT-suspension via a dialysis bag was seen to be 34.52 ± 1.19% (Figure 3). The drug release

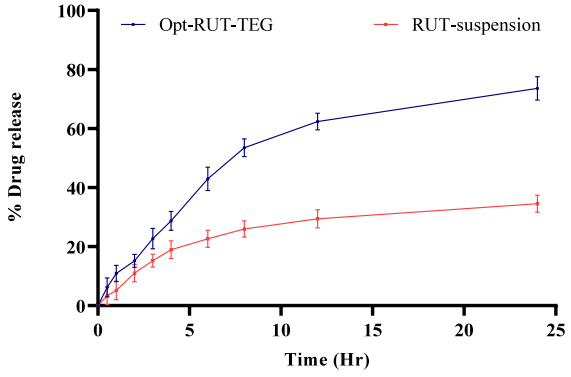

Figure 3. Comparative *in vitro* drug release of Opt-RUT-TE and RUT-suspension ($p < 0.0001$).

from Opt-RUT-TE is significantly higher ($p < 0.0001$) than the drug release from the suspension. The observed increase in drug release from Opt-RUT-TE can be due to the improved penetration aided by the smaller size of the vesicles and the greater solubility of the drug in transethosome. Various mathematical kinetic models, including zeroth order, first order, Higuchi, and Korsmeyer-Peppas models, were employed to fit the data obtained from the *in vitro* drug release experiment. The study observed the Higuchi matrix model exhibiting the correlation coefficient ($R^2 = 0.9497$), followed by the first-order model ($R^2 = 0.9239$) and the zeroth-order model, which had the lowest R^2 value ($R^2 = 0.8253$). Consequently, Higuchi's model was determined to be the most suitable model for the Opt-RUT-TE, as it exhibited the highest correlation coefficient value. The coefficient of determination (R^2) was determined to be 0.9742 through the application of the Korsmeyer-Peppas model to fit the data and analyze the release mechanism of RUT from Opt-RUT-TE. The study determined that the value of n falls between the range of 0 to 0.5 (n = 0.6879), suggesting that the release of RUT from optimized RUT-TE exhibits non-Fickian diffusion.

2.5. Evaluation of Gel. The Opt-RUT-TEG that was synthesized underwent an evaluation for several parameters. The gel exhibited a pleasing and uniform visual aspect, devoid of any granular particles. The pH values of the gel were determined to be 5.97 ± 0.69. The achieved pH level is

https://doi.org/10.1021/acsomega.4c01718
ACS Omega 2024, 9, 27300−27311

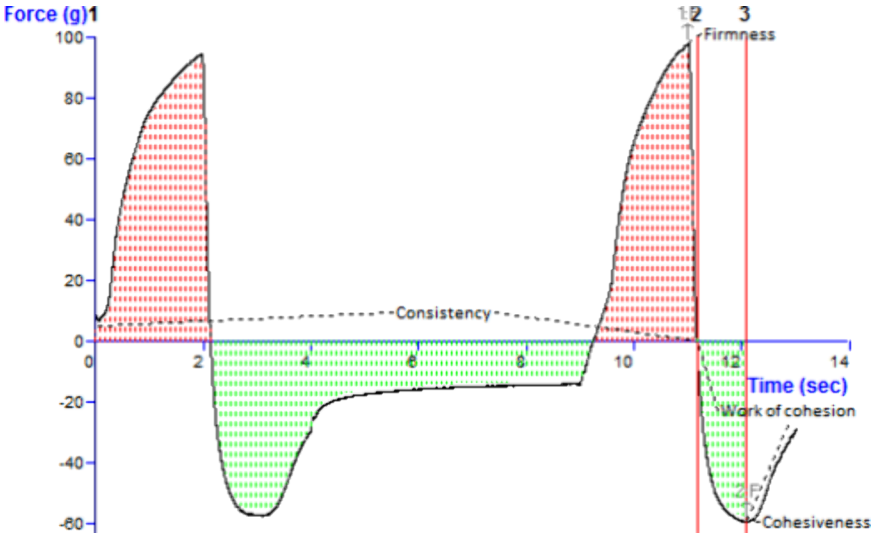

Figure 4. Texture analysis of Opt-RUT-TEG.

deemed to be within a safe range to mitigate the potential risk of skin irritation when the product is applied. The uniform distribution and patient compliance of gel formulations are dependent on two essential parameters: spreadability and extrudability. The gel exhibited a spreadability of 61.23 ± 3.17 g·cm/s and an extrudability of 49.74 ± 5.14 g/cm^2. Concurrently, the percentage of drug content in the nanogel was determined to be 92.78 ± 2.01%. The result indicated that the drug content was within the prescribed range of 100 ± 10%. This suggests that the drug was uniformly dispersed throughout the resulting formulation. Viscosity is a crucial physical characteristic of topical preparations that significantly affects the release of the drug. The viscosity of the gel was found to be 6109.49 ± 319.49 cP. The viscosity also affects the stability, spreadability, drug release, and ease of application of dosage forms.[43] Texture analysis of Opt-RUT-TEG (Figure 4) showed a firmness (g) of 98.14, a consistency (g·s) of 79.64, a cohesiveness (g) of −59.77, and a work of cohesion (g·s) of −44.23.

2.6. *Ex Vivo* Permeation Study. Figure 5 illustrates the comparative permeation of RUT from the optimized formula of Opt-RUT-TEG in relation to RUT-suspension gel over a period of 24 h. The results indicate that the optimized formula exhibited a higher permeation ($p < 0.0001$) of RUT (935.25 ± 10.49 μg/cm^2) compared to the RUT-suspension gel (522.57 ± 6.79 μg/cm^2) after 24 h, yielding a flux of approximately 0.0108 μg/cm^2/s for the optimized formulation. This suggests that RUT, when formulated optimally, may possess the ability to surpass the stratum corneum barrier more effectively and penetrate deeper layers of the skin. The observed behavior might be related to the inclusion of ethanol in the TE, which serves as a penetration enhancer. This property allows the TE to exhibit flexibility and consequently facilitates its high penetration.[44] According to the findings, TE exerts both pull and push actions on the intercellular interface of the stratum corneum (SC) cells, potentially leading to increased drug penetration. The push effect refers to a thermodynamic phenomenon observed during the evaporation of ethanol. On the other hand, the pull effect is a consequence of ethanol interacting with SC lipids, leading to the creation of supplementary pathways for penetration.[44] It is important to mention that Opt-RUT-TE had superior permeability characteristics, as seen by a flux value of 34.36 μg/cm^2/h (approximately 0.0095 μg/cm^2/s), in contrast to the 19.49 μg/cm^2/h (approximately 0.0054 μg/cm^2/s) observed for the RUT-suspension gel. The enhancement ratio, calculated as the ratio of flux values, indicates an approximately 1.759-fold enhancement in permeability for the optimized formulation compared to that of the RUT-suspension gel.

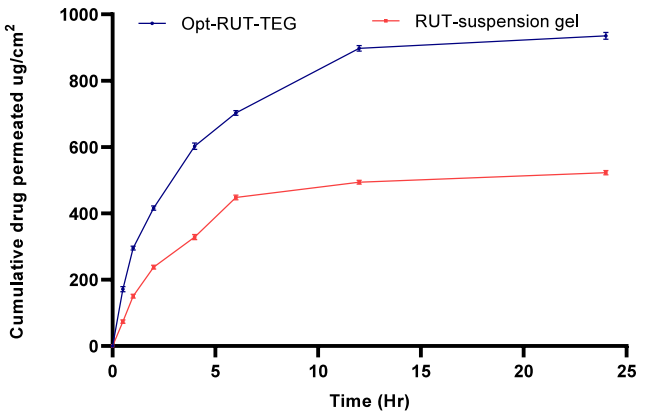

Figure 5. Comparative skin permeation of Opt-RUT-TE and RUT-suspension gel ($p < 0.0001$).

2.7. Tape Stripping. The tape stripping method was used to assess the penetration of RUT in stratum-corneum and epidermis-dermis layers of the skin. The results indicated that the RUT-suspension gel exhibited significantly higher retention in the stratum corneum (703.97 ± 16.80 μg/cm^2) compared to that of the Opt-RUT-TE gel formulation (152.11 ± 34.69 μg/cm^2), whereas the Opt-RUT-TE gel formulation showed a higher concentration in the epidermis-dermis (562.30 ± 46.00 μg/cm^2) compared to that of the RUT-suspension gel (83.12 ± 14.42 μg/cm^2) as shown in Figure 6. Statistical analysis confirmed the significant difference ($p < 0.0001$) between the Opt-RUT-TE gel and the RUT-suspension gel. This validates the potential of the Opt-RUT-TE gel for achieving enhanced drug levels in the subcutaneous layer, with reduced penetration into deeper skin layers, which is essential for topical drug delivery systems. The slower penetration of the developed formulation may lead to reduced systemic toxicity. Addition-

https://doi.org/10.1021/acsomega.4c01718
ACS Omega 2024, 9, 27300−27311

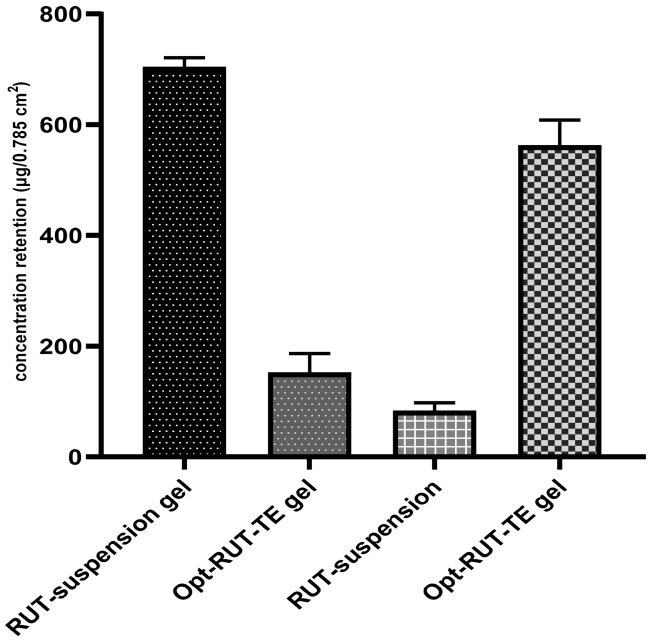

Figure 6. Comparative RUT-retention by tape-stripping from Opt-RUT-TEG and RUT-suspension gel in stratum corneum and epidermis-dermis skin layers ($p < 0.0001$).

ally, the study's findings, which showed the drug residing primarily on the top of the dermal layer, suggest an improved therapeutic drug profile for treating microbial infections. Enhanced topical bioavailability can be attributed to various mechanisms, including increased solubility due to RUT transformation, penetration enhancement properties of sodium cholate, high lipid interaction modifying the stratum corneum structure, and enhanced thermodynamic activity. Overall, both the permeation and tape stripping studies demonstrated the superiority of the Opt-RUT-TE gel over the RUT-suspension gel, indicating enhanced penetration and targeted delivery of RUT to the superficial skin layers, thereby potentially improving the efficacy for treating cutaneous conditions.[45,46]

2.8. Antimicrobial Activity. Figure 7 illustrates the outcomes of the antibacterial efficacy of the produced Opt-RUT-TEG and RUT-suspension gel against *S. aureus* (Gram-positive bacterium). The cup−plate technique was employed to measure the zone of inhibition. The findings demonstrated

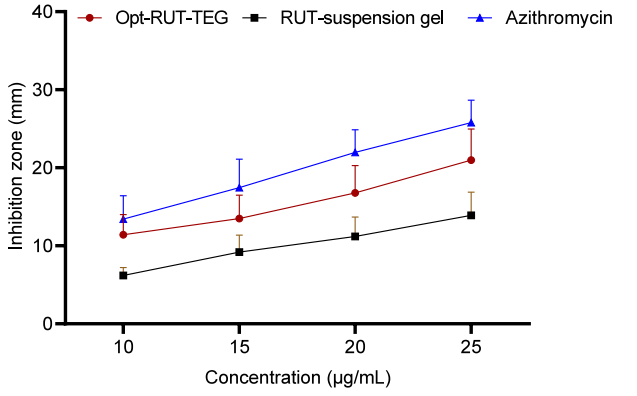

Figure 7. Comparative antimicrobial activity of Opt-RUT-TEG and RUT-suspension gel with the standard formulation (azithromycin) showing the inhibition zone (mm) ($p < 0.0001$).

the efficacy of Opt-RUT-TEG against *S. aureus*, with a zone of inhibition that was substantially larger than that of the RUT-suspension gel ($p < 0.0001$). The Opt-RUT-TEG and standard (azithromycin) displayed inhibition zones of 20.99 ± 3.97 and 25.78 ± 2.87 mm, whereas the RUT-suspension gel displayed an inhibition zone of 13.89 ± 2.99 mm. The findings indicate that there is a steady decline in organism viability in a dose-dependent way as the concentration of RUT increases. Rutin has been well examined for its antibacterial properties against a wide range of bacterial species. It has exhibited a significant level of inhibition of the growth of bacteria.[47] As rutin is a flavonoid, it is widely recognized for its ability to combat various harmful microorganisms as antibacterial agents. The suggested antibacterial mechanisms of flavonoids encompass the repression of nucleic acid synthesis, disturbance of cytoplasmic membrane function, hindrance of energy metabolism, prevention of attachment and biofilm formation, inhibition of porin activity on the cell membrane, and modification of membrane permeability.[48] Furthermore, the enhanced antibacterial efficacy of Opt-RUT-TEG may be attributed to the synergistic antibacterial effect of PEG 400 and the nanosystems of the ethosome vesicles. PEG 400 has significant antimicrobial properties against various pathogenic microorganisms,[49] while delivery systems such as nanoparticles offer advantages in terms of greater intracellular absorption compared to that of microparticles. Moreover, their minuscule dimensions and considerable mobility make them well-suited for drug targeting.[50] The existence of ethanol and phospholipids plays a vital role in impeding bacterial development since they both compromised the structural integrity of the bacteria's cell wall. As a result, ethosomes could effectively permeate the bacterial cytoplasmic membrane and achieve an ideal concentration.[23]

2.9. Stability. The physical attributes were examined for a span of 6 months at temperatures of 25 ± 2 °C/60 ± 5% RH. The results are presented in Table 3. The results of our study showed no considerable changes in the uniformity, color, pH, spreadability, vesicle size, and entrapment efficiency after a storage period of 6 months at either temperature.

3. CONCLUSIONS

The current study effectively showcased the development and optimization of rutin-loaded transethosomes using a quality by design (QbD) technique. The formulated transethosomes exhibited favorable attributes, including the nanovesicle size (<200 nm), a low polydispersity index (<0.3), and a negative zeta potential, indicative of their stability and potential for skin permeation. Transmission electron microscopy confirmed their spherical morphology, validating their suitability for dermal delivery. The optimized formulation (Opt-RUT-TE) demonstrated significantly higher drug release compared to that of the RUT-suspension, indicating its potential for improved therapeutic efficacy. The conversion of the transethosomal formulation to a gel further enhanced its applicability to skin applications. The Opt-RUT-TE gel exhibited substantially higher drug permeation through the rat skin compared to the RUT-suspension gel, highlighting its superior skin penetration capability.

Beyond enhanced permeation, the transethosomal gel exhibited promising antibacterial activity, particularly against Gram-positive bacteria, with Opt-RUT-TE gel showing a higher inhibition zone compared to that of the RUT-suspension gel. This dual functionality underscores the

https://doi.org/10.1021/acsomega.4c01718
ACS Omega 2024, 9, 27300−27311

Table 3. Stability Studies of Opt-RUT-TE and Opt-RUT-TE Gel at Room Temperature (25 ± 2 °C/60 ± 5% RH)

Time (months)	0	2	4	6
Opt-RUT-TE Gel				
Homogeneity	Homogeneous			
pH	5.89 ± 1.09	5.78 ± 0.87	5.98 ± 1.14	5.97 ± 0.61
Color	Slightly yellowish			
Spreadability	*a*	*a*	*a*	*b*
Extrudability	*a*	*a*	*b*	*a*
Opt-RUT-loaded TE				
Physical appearance	No change in appearance			
Vesicle size (nm)	161.24 ± 0.79	162.78 ± 1.98	163.54 ± 1.49	164.49 ± 2.01
Entrapment efficiency (%)	83.98 ± 2.49	83.91 ± 1.47	83.11 ± 2.04	81.78 ± 1.97

[a]Excellent. [b]Satisfactory.

therapeutic potential of rutin-loaded transethosomal gel in treating dermatological diseases, offering improved skin permeability and antibacterial effects.

However, further research is warranted to explore potential adverse effects and optimize the efficacy of formulations in clinical studies. Overall, this study contributes valuable insights to the therapeutic possibilities of rutin-loaded transethosomal gel formulations for dermatological conditions.

4. EXPERIMENTAL SECTION

4.1. Materials. The rutin (≥94% (HPLC) compound was acquired from Sigma-Aldrich Chemical Co. located in St. Louis, MO, USA. Phospholipid 90G and sodium cholate were acquired from Gattefossé, a French business located in Saint-Priest. The dialysis membrane employed in the experiment is a cellulose membrane obtained from Sigma-Aldrich Chemical Co. in St. Louis, MO, USA. The membrane has a molecular weight cut off range of 12,000−14,000 Da. The rodent albino rat skin was purchased from Etsy Pvt. Ltd. India. Carbopol 934, poly(ethylene glycol) 400, glycerin, and triethanolamine were obtained from El-Nasr Pharmaceutical Company in Cairo, Egypt. The ethanol was obtained from Fisher Scientific, situated in Loughborough, U.K. All of the remaining materials exhibited a high level of purity.

4.2. Design of Experimental Study. The response surface model was created using Design Expert software (version 13, Stat-Ease Inc., Minneapolis, MN, USA) by applying various combinations of parameters. A Box-Behnken design (BBD) consisting of three variables and levels was utilized to generate numerous transethosomal (TE) formulations. The study examined the impact of three independent parameters, namely, lipid concentration (mg, A), sodium cholate (mg, B), and ethanol (mL, C) on dependent variables such as the entrapment efficiency (%, Y_1) and cumulative drug permeation (Y_2) as presented in Table 4. The independent components were evaluated at different levels (−1, 0, 1). Table 4 presents a concise overview of the experimental design pattern used in the Box-Behnken design. The estimation of model and term significance was conducted using the analysis of variance (ANOVA). The significance of probability p values is often denoted when they are less than 0.05. Three-dimensional surface plots were created to establish a correlation among the results obtained from the statistical analysis.

Table 4. Optimization by Utilizing the Box-Behnken Design for RUT-Loaded Transethosome

	Levels		
Independent parameters	Lowest	Medium	Highest
Phospholipid 90G (mg)	120	140	160
Sodium cholate (mg)	10	20	30
Ethanol (mL)	7	11	15
Dependent factors	Aim		
Entrapment efficiency (% EE)	Maximum		
Drug permeation ($\mu g/cm^2$)	Maximum		

4.2.1. Preparation of Rutin-Loaded Transethosomes (RUT-TE). Using a rotary evaporator, transethosomes of rutin (RUT-TE) were developed. After the specified amounts of phospholipid 90G, RUT, and sodium cholate were dissolved in a 6:2 v/v solution of chloroform and methanol, the mixture was poured into a round-bottom flask. The rotary evaporator was used to evaporate the organic solvents at low pressure and under vacuum, following the formation of a thin layer of the lipid mixture in the round-bottomed flask. The lipid film was suitable for use after 4 h of vacuuming the film to eliminate any remaining solvent residue. The lipid film was allowed to air dry before being rehydrated in a hydroethanolic solution for 1 h. This solution was then added to the round-bottomed flask containing the thin film and chilled to cause enough swelling.[51] Transethosomes were next produced by ultrasonically sonicating the dispersions for 2 min in an ultrasonicator (UP100H, Hielscher Ultrasonics GmbH, Berlin, Germany).

4.3. Characterization of Developed RUT-TE. *4.3.1. Entrapment Efficiency and Drug-Loading Percentage.* A predetermined volume of an Opt-RUT-TE dispersion (2 mL) was deposited in a centrifuge tube and subjected to centrifugation at an average speed of 18,000 rpm for 20 min at a temperature of 4 °C, utilizing a cooling centrifuge (Remi Instruments, Pvt. Ltd., India) for assistance. The liquid portion was isolated and analyzed by using spectrophotometry at a wavelength of 260 nm with a Shimadzu 1800 spectrophotometer manufactured in Japan. This analysis was performed to determine the amount of unentrapped drug present.[52] The calculations of percent entrapment efficiency and drug loading were performed according to the equations below, respectively.

$$\%\ \text{Entrapment efficiency} = \frac{\text{Total amount of RUT entrapped}}{\text{Total amount of RUT added}} \times 100$$

$$\%\ \text{Drug loading} = \frac{\text{Amount of drug entrapped}}{\text{Amount of drug and lipid}} \times 100$$

https://doi.org/10.1021/acsomega.4c01718
ACS Omega 2024, 9, 27300−27311

4.3.2. Vesicle Size, PDI, and Zeta Potential. The vesicle size, polydispersity index (PDI), and zeta potential were determined through the utilization of the dynamic light scattering (DLS) technique. The samples were appropriately diluted with deionized water and analyzed using a Zetasizer Nano ZS instrument (Malvern Instruments Ltd., Worcestershire, U.K.). The measurements were conducted three times, and the outcomes were expressed as the average diameter (Z average) together with the standard deviation (SD).[53]

4.3.3. Transmission Electron Microscopy. The surface morphology of Opt-RUT-TE was examined by using a Morgagni 268D transmission electron microscope (TEM) (FEI, MA). A small amount of TE solution was applied to a grid coated with carbon. The sample was subsequently treated with a phosphotungstic acid stain for a duration of 10 s. Following this, the sample was left to dry naturally at room temperature and was then examined using a transmission electron microscope (TEM).[54]

4.4. *In Vitro* Drug Release. The *in vitro* drug release of Opt-RUT-TE and RUT-suspension was evaluated by using the dialysis bag diffusion method. A 2 mg dose of RUT was mixed with 2 mL of phosphate-buffered saline (PBS 7.4) to prepare RUT-suspension. The suspension and Opt-RUT-TE were then placed inside a dialysis bag, with both sides of the bag securely knotted. The dialysis bag, together with its contents, was immersed in a beaker containing 20 mL of pH 7.4 PBS, which served as the release medium. The beaker was positioned on a magnetic stirrer (Stuart, SB161, U.K.) operating at a speed of 50 rpm. The temperature was carefully controlled at 37 ± 1 °C for the duration of the experiment. The release medium was periodically replaced at specific time intervals (2, 4, 6, 8, and 24 h) with an equivalent volume of fresh PBS. The quantity of the drug that was released was evaluated using spectrophotometric analysis at a wavelength of 260 nm using a UV−vis spectrophotometer. The experiment was conducted in triplicate, with multiple samples being examined for each measurement, and the mean plus standard deviation (SD) was calculated.[55]

4.5. Preparation of Rutin-Loaded Transethosomal Gel. In order to enhance the rheological properties of the gel, Carbopol 974P (1 wt %) was employed as a supplementary carrier. Carbopol 974P was introduced into distilled water while maintaining continuous agitation and thereafter placed in a dark environment for a duration of 24 h to achieve complete swelling. Subsequently, the addition components such as glycerin and polyethylene glycol 400 (PEG) (15% w/w) were used as a humectant, and the addition of triethanolamine was carried out in a gradual manner until the formation of a gel that is both visually transparent and has desirable rheological properties. Following gel formation, Opt-RUT-TE was incrementally introduced and agitated to ensure thorough homogenization.[56]

4.6. Characterization of Optimized Rutin-Loaded Transethosomal Gel (Opt-RUT-TEG). *4.6.1. Homogeneity, pH, and Drug Content.* The color, transparency, grittiness, and homogeneity of the prepared Opt-RUT-TEG were assessed by applying the gel to transparent paper or to a glass slide. The formulation's pH was determined by the utilization of a pH meter (PCT-407 portable pH Meter, Taipei City, Taiwan). To determine the drug content, a mixture was prepared by combining 1 g of Opt-RUT-TEG with 100 mL of distilled water. The drug's composition was analyzed using spectrophotometry at a wavelength of 260 nm, comparing it to a blank sample that included the same components but without the drug.[57]

4.6.2. Spreadability and Extrudability. To conduct a study of the efficiency of gel formulations in terms of spreadability, a measured amount of the gel sample was deposited onto a glass slide. Another glass slide was then positioned on top of the gel, effectively enclosing the sample between the two glass slides. Subsequently, the specimens were subjected to compression between the upper and lower glass slides, employing a force of 100*g*, resulting in the formation of a uniform thin layer. A fraction of the surplus material was subsequently eliminated. The upper glass slide was successfully detached with ease following its attachment to a 20 g weight, while the other slide remained firmly affixed to the platform with no disturbance. The spreadability of the upper glass was determined by measuring the duration required to move it a distance of 7.50 cm across the thin sheet positioned on the lower glass slide. In order to assess the extrudability of the gel formulations that were created, the quantity of gel that was expelled from the collapsible tubes was examined. A predetermined quantity of nanogel formulations was measured and subsequently deposited in collapsible tubes. Then the extrudability of the formulations from the collapsible tubes was determined by measuring the weight (in grams) required to extrude a 1 cm ribbon, expressed as g cm^{-2}.[58]

4.6.3. Viscosity Measurement and Texture Analysis. The viscosity of the transethosomal gel was measured at a temperature of 25 ± 1 °C using a Brookfield viscometer (model DV-II, spindle number 02, Middleboro, MA, USA). A fraction of the gel formulation was transferred to a beaker and allowed to settle at ambient temperature for a duration of 30 min. The spindle was inserted into the mixture without making contact with the bottom of the beaker and rotated at a speed of 20 rpm. The viscosity was measured and recorded in centipoise (cP).[59] The instrumental texture profile analysis (TPA) was performed using a stable microsystems texture analyzer (model TA-XT2; StableMicrosystems Ltd., Godalming, Surrey, U.K.). The texture analyzer was connected to the computer software known as "texture expert". The gel was incorporated into a 100 mL beaker evenly without the formation of any bubbles. Prior to experiment, the equipment was automatically calibrated to zero, specifically when the top plate made contact with the surface of the gel.[60]

4.6.4. Ex Vivo Skin Permeation. In this investigation, a Franz diffusion cell with a diffusion area of 1.76 cm^2 was employed, demonstrating its efficacy and efficiency. The rodent albino rat skin (1 cm^2) was positioned onto the diffusion cell, ensuring that the dermal side was in contact with the receptor phase. A diffusion medium of 10 mL, specifically pH 7.4 phosphate-buffered saline (PBS), was introduced into the receptor compartment. Subsequently, the medium underwent a reduction in stirring intensity with the magnetic stirrer operating at 100 rpm (rpm). The system was maintained at an equilibrium temperature of 37 ± 0.5 °C. Approximately 20 mg of gel was administered and evenly distributed across the designated diffusion area on the skin. The estimation process involved extracting the sample solution from the receptor compartment at specific time intervals as mentioned in the *in vitro* study and replacing it with a fresh buffer medium. Each trial was conducted over a 24 h period (0, 0.5, 1, 2, 4, 6, 8, 12, and 24 h), during which the permeation of drug released via the skin was determined using UV spectrophotometry at 260 nm.[61]

https://doi.org/10.1021/acsomega.4c01718
ACS Omega 2024, 9, 27300−27311

4.7. Tape Stripping Method. The method of tape stripping was employed to assess the levels of RUT from Opt-RUT-TEG and RUT-suspension gel accumulated within the stratum corneum-epidermis and epidermis-dermis layers of the skin, as carried out by Bolla et al.[45] Upon completion of skin permeation studies, the skin samples were delicately removed from the cells and positioned on a flat surface to expose the diffusion area. Any excess formulation present on the skin surface was gently eliminated by softly rubbing the skin with tissue. The stratum corneum and portions of the epidermis layers were then isolated by using 3M Scotch Magic tape. Precut pieces of tape were pressed onto the skin and promptly removed with forceps to strip away the stratum corneum (with the initial strip being discarded). Typically, an average of 10 strips were needed to entirely remove the stratum corneum. The remaining epidermis-dermis layers of the skin were subsequently diced into small fragments using sterile surgical scissors. All of the strips (excluding the first) and skin fragments were transferred to a conical tube containing 10 mL of methanol for RUT extraction. The extraction process involved sonication in an ultrasonic water bath for 30 min, followed by overnight incubation at 4 °C. Postextraction, the resulting solution underwent centrifugation for 30 min at 15,000 rpm, and the drug content in the supernatant was evaluated using a UV spectrophotometer.[45]

4.8. Antimicrobial Activity. The present study aimed to assess the antibacterial efficacy of the standard (azithromycin), Opt-RUT-TEG, and RUT-suspension gel by the cup−plate technique, targeting the inhibition of *Staphylococcus aureus* (*S. aureus*) growth. The cup−plate approach was employed in accordance with the experimental methodology conducted by El Atki et al., with specific alterations.[62] The plates underwent an initial sterilization process lasting 60 min in a hot air oven set at a temperature of 160 °C. Subsequently, 10 mL of sterile nutritional agar medium, which had undergone sterilization for a duration of 15 min at a temperature of 121 °C in an autoclave, was dispensed onto each plate. The plates were allowed to undergo solidification in a sterile environment, after which the microorganism was introduced into the plates.[63] Three cups, each with a diameter of 3 mm, were fabricated on the plate by using a cork borer. Subsequently, the samples were introduced into the cups to assess their effectiveness. The plates were thereafter placed in an incubator set at a temperature of 25 °C for a duration of 24 h. Following incubation, the zone of inhibition for each preparation was evaluated using a graduated scale, and the results were subsequently compared.

4.9. Stability. To assess the stability of Opt-RUT-TEG, the formulation was stored at a temperature of 25 ± 2 °C/60 ± 5% RH for a duration of 6 months. The samples were collected in a systematic manner at regular intervals of 0, 2, 4, and 6 months. Each sample was subjected to triplicate analysis to assess visual characteristics, physical appearance, vesicle size, entrapment efficiency, pH levels, spreadability, and extrudability.[58,64]

4.10. Statistical Analysis. The data obtained were presented as means ± the standard deviation (n = 3). The statistical analysis employed the use of one-way ANOVA, utilizing GraphPad Prism version 8. A statistically significant difference was considered when the p value was less than 0.05 and 0.0001.

■ ASSOCIATED CONTENT

Data Availability Statement

All data is available throughout the manuscript.

■ AUTHOR INFORMATION

Corresponding Author

Mohd Imran − *R&D Executive, Aimil Pharmaceutical, New Delhi 110028, India;* orcid.org/0000-0001-7349-3019; Email: imranidrisi00786@gmail.com

Authors

Mohammed F. Aldawsari − *Department of Pharmaceutics, College of Pharmacy, Prince Sattam Bin Abdulaziz University, Al-kharj 11942, Saudi Arabia*

Aftab Alam − *Department of Pharmacognosy, College of Pharmacy, Prince Sattam Bin Abdulaziz University, Al-Kharj 11942, Saudi Arabia*

Complete contact information is available at: https://pubs.acs.org/10.1021/acsomega.4c01718

Author Contributions

Mohammed F. Aldawsari: Conceptualization, methodology, validation, resources, review and editing, and funding acquisition. Aftab Alam: Conceptualization, software, writing and original draft preparation, and supervision. Mohd Imran: Methodology, formal analysis, investigation, review, and editing.

Notes

Institutional Review Board Statement: Prince Sattam bin Abdulaziz University has been approved.

The authors declare no competing financial interest.

■ ACKNOWLEDGMENTS

This study is supported via funding from Prince Sattam bin Abdulaziz University Project Number (PSAU/2024/R/1445).

■ REFERENCES

(1) Balkrishnan, R.; Manuel, J.; Feldman, S. R.; Rapp, S. R. Measurement of Health-Related Quality of Life (HRQOL) Associated with Skin Disease. *J. Am. Acad. Dermatol.* **2004**, *51* (1 suppl), 3.

(2) Vos, T.; et al. Global, Regional, and National Incidence, Prevalence, and Years Lived with Disability for 310 Diseases and Injuries, 1990−2015: A Systematic Analysis for the Global Burden of Disease Study 2015. *Lancet (London, England)* **2016**, *388* (10053), 1545−1602.

(3) Tognetti, L.; Martinelli, C.; Berti, S.; Hercogova, J.; Lotti, T.; Leoncini, F.; Moretti, S. Bacterial Skin and Soft Tissue Infections: Review of the Epidemiology, Microbiology, Aetiopathogenesis and Treatment: A Collaboration between Dermatologists and Infectivologists. *Journal of the European Academy of Dermatology and Venereology.* **2012**, *26*, 931.

(4) Tong, S. Y. C.; Davis, J. S.; Eichenberger, E.; Holland, T. L.; Fowler, V. G. Staphylococcus Aureus Infections: Epidemiology, Pathophysiology, Clinical Manifestations, and Management. *Clin. Microbiol. Rev.* **2015**, *28* (3), 603.

(5) Abruzzo, A.; Parolin, C.; Rossi, M.; Vitali, B.; Cappadone, C.; Bigucci, F. Development and Characterization of Azithromycin-Loaded Microemulsions: A Promising Tool for the Treatment of Bacterial Skin Infections. *Antibiotics* **2022**, *11* (8), 1040.

(6) Selvaraj, K.; Chowdhury, R.; Bhattacharjee, C. Isolation and Structural Elucidation of Flavonoids from Aquatic Fern Azolla Microphylla and Evaluation of Free Radical Scavenging Activity. *Int. J. Pharm. Pharm. Sci.* **2013**, *5*, 743749.

(7) Kunjiappan, S.; Theivendran, P.; Baskararaj, S.; Sankaranarayanan, B.; Palanisamy, P.; Saravanan, G.; Arunachalam, S.; Sankaranarayanan, M.; Natarajan, J.; Somasundaram, B.; Wadhwani, A. Modeling a PH-Sensitive Zein-Co-Acrylic Acid Hybrid Hydrogels Loaded 5-Fluorouracil and Rutin for Enhanced Anticancer Efficacy by Oral Delivery. *3Biotech* **2019**, *9* (5), DOI: 10.1007/s13205-019-1720-x.
(8) Choi, J. K.; Kim, S. H. Rutin Suppresses Atopic Dermatitis and Allergic Contact Dermatitis. *Exp. Biol. Med.* **2013**, *238* (4), 410.
(9) Alonso, C.; Rubio, L.; Touriño, S.; Martí, M.; Barba, C.; Fernández-Campos, F.; Coderch, L.; Luís Parra, J. Antioxidative Effects and Percutaneous Absorption of Five Polyphenols. *Free Radic. Biol. Med.* **2014**, *75*, 149.
(10) Arjumand, W.; Seth, A.; Sultana, S. Rutin Attenuates Cisplatin Induced Renal Inflammation and Apoptosis by Reducing NFκB, TNF-α and Caspase-3 Expression in Wistar Rats. *Food Chem. Toxicol.* **2011**, *49* (9), 2013.
(11) Alonso-Castro, A. J.; Domínguez, F.; García-Carrancá, A. Rutin Exerts Antitumor Effects on Nude Mice Bearing SW480 Tumor. *Arch. Med. Res.* **2013**, *44* (5), 346.
(12) Ganeshpurkar, A.; Bansal, D.; Dubey, S.; Dubey, N. Experimental Studies on Bioactive Potential of Rutin. *Chronicles Young Sci.* **2013**, *4* (2), 153.
(13) Tao, J.; Hu, Q.; Yang, J.; Li, R.; Li, X.; Lu, C.; Chen, C.; Wang, L.; Shattock, R.; Ben, K. In Vitro Anti-HIV and -HSV Activity and Safety of Sodium Rutin Sulfate as a Microbicide Candidate. *Antiviral Res.* **2007**, *75* (3), 227.
(14) Pandian, S. R. K.; Pavadai, P.; Vellaisamy, S.; Ravishankar, V.; Palanisamy, P.; Sundar, L. M.; Chandramohan, V.; Sankaranarayanan, M.; Panneerselvam, T.; Kunjiappan, S. Formulation and Evaluation of Rutin-Loaded Solid Lipid Nanoparticles for the Treatment of Brain Tumor. *Naunyn. Schmiedebergs. Arch. Pharmacol.* **2021**, *394* (4), 735.
(15) Satari, A.; Ghasemi, S.; Habtemariam, S.; Asgharian, S.; Lorigooini, Z. Rutin: A Flavonoid as an Effective Sensitizer for Anticancer Therapy; Insights into Multifaceted Mechanisms and Applicability for Combination Therapy. *Evidence-based Complementary and Alternative Medicine.* **2021**, *2021*, 1.
(16) Wang, Y. F.; Ni, Z. Y.; Dong, M.; Cong, B.; Shi, Q. W.; Gu, Y. C.; Kiyota, H. Secondary Metabolites of Plants from the Genus Saussurea: Chemistry and Biological Activity. *Chemistry and Biodiversity.* **2010**, *7*, 2623.
(17) Cushnie, T. P. T.; Lamb, A. J. Detection of Galangin-Induced Cytoplasmic Membrane Damage in Staphylococcus Aureus by Measuring Potassium Loss. *J. Ethnopharmacol.* **2005**, *101* (1−3), 243.
(18) Miklasińska-Majdanik, M.; Kępa, M.; Wąsik, T. J.; Zapletal-Pudełko, K.; Klim, M.; Wojtyczka, R. D. The Direction of the Antibacterial Effect of Rutin Hydrate and Amikacin. *Antibiotics* **2023**, *12* (9), 1469.
(19) Amin, M. U.; Khurram, M.; Khattak, B.; Khan, J. Antibiotic Additive and Synergistic Action of Rutin, Morin and Quercetin against Methicillin Resistant Staphylococcus Aureus. *BMC Complement. Altern. Med.* **2015**, *15* (1), DOI: 10.1186/s12906-015-0580-0.
(20) Gullón, B.; Lú-Chau, T. A.; Moreira, M. T.; Lema, J. M.; Eibes, G. Rutin: A Review on Extraction, Identification and Purification Methods, Biological Activities and Approaches to Enhance Its Bioavailability. *Trends in Food Science and Technology.* **2017**, *67*, 220.
(21) Bellefroid, C.; Lechanteur, A.; Evrard, B.; Mottet, D.; Debacq-Chainiaux, F.; Piel, G. In Vitro Skin Penetration Enhancement Techniques: A Combined Approach of Ethosomes and Microneedles. *Int. J. Pharm.* **2019**, *572*, 118793.
(22) De Gaetano, F.; Cristiano, M. C.; Venuti, V.; Crupi, V.; Majolino, D.; Paladini, G.; Acri, G.; Testagrossa, B.; Irrera, A.; Paolino, D.; Tommasini, S.; Ventura, C. A.; Stancanelli, R. Rutin-Loaded Solid Lipid Nanoparticles: Characterization and in Vitro Evaluation. *Molecules* **2021**, *26* (4), 1039.
(23) Paiva-Santos, A. C.; Silva, A. L.; Guerra, C.; Peixoto, D.; Pereira-Silva, M.; Zeinali, M.; Mascarenhas-Melo, F.; Castro, R.; Veiga, F. Ethosomes as Nanocarriers for the Development of Skin Delivery Formulations. *Pharm. Res.* **2021**, *38*, 947.
(24) Mombeiny, R.; Tavakol, S.; Kazemi, M.; Mehdizadeh, M.; Hasanzadeh, A.; Karimi Babaahmadi, M.; Abedi, A.; Keyhanvar, P. Anti-Inflammatory Ethosomal Nanoformulation in Combination with Iontophoresis in Chronic Wound Healing: An Ex Vivo Study. *IET Nanobiotechnology* **2021**, *15* (9), 710.
(25) Aodah, A. H.; Hashmi, S.; Akhtar, N.; Ullah, Z.; Zafar, A.; Zaki, R. M.; Khan, S.; Ansari, M. J.; Jawaid, T.; Alam, A.; Ali, M. S. Formulation Development, Optimization by Box−Behnken Design, and In Vitro and Ex Vivo Characterization of Hexatriacontane-Loaded Transethosomal Gel for Antimicrobial Treatment for Skin Infections. *Gels* **2023**, *9* (4), 322.
(26) Slavkova, M.; Tzankov, B.; Popova, T.; Voycheva, C. Gel Formulations for Topical Treatment of Skin Cancer: A Review. *Gels.* **2023**, *9*, 352.
(27) Ghazwani, M.; Alqarni, M. H.; Hani, U.; Alam, A. QbD-Optimized, Phospholipid-Based Elastic Nanovesicles for the Effective Delivery of 6-Gingerol: A Promising Topical Option for Pain-Related Disorders. *Int. J. Mol. Sci.* **2023**, *24* (12), 9983.
(28) Kamel, R.; Mostafa, D. M. Rutin Nanostructured Lipid Cosmeceutical Preparation with Sun Protective Potential. *J. Photochem. Photobiol. B Biol.* **2015**, *153*, 59.
(29) Cândido, T. M.; De Oliveira, C. A.; Ariede, M. B.; Velasco, M. V. R.; Rosado, C.; Baby, A. R. Safety and Antioxidant Efficacy Profiles of Rutin-Loaded Ethosomes for Topical Application. *AAPS PharmSciTech* **2018**, *19* (4), 1773.
(30) Sahu, A. K.; Kumar, T.; Jain, V. Formulation Optimization of Erythromycin Solid Lipid Nanocarrier Using Response Surface Methodology. *Biomed Res. Int.* **2014**, *2014*, 1.
(31) Lala, R. R.; Shinde, A. S. Development, Optimization, and in Vitro Evaluation of Atorvastatin Calcium and Vinpocetine Codelivery by Solid Lipid Nanoparticles for Cancer Therapy. *Futur. J. Pharm. Sci.* **2021**, *7* (1), DOI: 10.1186/s43094-021-00351-y.
(32) Mahmood, S.; Taher, M.; Mandal, U. K. Experimental Design and Optimization of Raloxifene Hydrochloride Loaded Nano-transfersomes for Transdermal Application. *Int. J. Nanomedicine* **2014**, *9*, 4331.
(33) Sultana, N.; Ali, A.; Waheed, A.; Jabi, B.; Yaqub khan, M.; Mujeeb, M.; Sultana, Y.; Aqil, M. Dissolving Microneedle Transdermal Patch Loaded with Risedronate Sodium and Ursolic Acid Bipartite Nanotransfersomes to Combat Osteoporosis: Optimization, Characterization, in Vitro and Ex Vivo Assessment. *Int. J. Pharm.* **2023**, *644*, 123335.
(34) Abdallah, M. H.; Lila, A. S. A.; Shawky, S. M.; Almansour, K.; Alshammari, F.; Khafagy, E. S.; Makram, T. S. Experimental Design and Optimization of Nano-Transfersomal Gel to Enhance the Hypoglycemic Activity of Silymarin. *Polymers (Basel).* **2022**, *14* (3), 508.
(35) El-Menshawe, S. F.; Ali, A. A.; Halawa, A. A.; Srag El-Din, A. S. G. A Novel Transdermal Nanoethosomal Gel of Betahistine Dihydrochloride for Weight Gain Control: In-Vitro and in-Vivo Characterization. *Drug Des. Devel. Ther.* **2017**, *11*, 3377.
(36) Akombaetwa, N.; Ilangala, A. B.; Thom, L.; Memvanga, P. B.; Witika, B. A.; Buya, A. B. Current Advances in Lipid Nanosystems Intended for Topical and Transdermal Drug Delivery Applications. *Pharmaceutics.* **2023**, *15*, 656.
(37) Iizhar, S. A.; Syed, I. A.; Satar, R.; Ansari, S. A. In Vitro Assessment of Pharmaceutical Potential of Ethosomes Entrapped with Terbinafine Hydrochloride. *J. Adv. Res.* **2016**, *7* (3), 453.
(38) Elsayed, M. M. A.; Abdallah, O. Y.; Naggar, V. F.; Khalafallah, N. M. Lipid Vesicles for Skin Delivery of Drugs: Reviewing Three Decades of Research. *Int. J. Pharm.* **2007**, *332*, 1.
(39) Clavijo-Romero, A.; Quintanilla-Carvajal, M. X.; Ruiz, Y. Stability and Antimicrobial Activity of Eucalyptus Essential Oil Emulsions. *Food Sci. Technol. Int.* **2019**, *25* (1), 24.
(40) Malik, S. N.; Canaham, D. H.; Gouda, M. W. Effect of Surfactants on Absorption through Membranes III: Effects of Dioctyl Sodium Sulfosuccinate and Poloxalene on Absorption of a Poorly Absorbable Drug, Phenolsulfonphthalein, in Rats. *J. Pharm. Sci.* **1975**, *64* (6), 987.

https://doi.org/10.1021/acsomega.4c01718
ACS Omega 2024, 9, 27300−27311

(41) Rahman, M.; Singh, J. G.; Afzal, O.; Altamimi, A. S. A.; Alrobaian, M.; Haneef, J.; Barkat, M. A.; Almalki, W. H.; Handa, M.; Shukla, R.; Nasar Mir Najib Ullah, S.; Kumar, V.; Beg, S. Preparation, Characterization, and Evaluation of Curcumin-Graphene Oxide Complex-Loaded Liposomes against Staphylococcus Aureus in Topical Disease. *ACS Omega* **2022**, *7* (48), 43499.
(42) Opatha, S. A. T.; Titapiwatanakun, V.; Chutoprapat, R. Transfersomes: A Promising Nanoencapsulation Technique for Transdermal Drug Delivery. *Pharmaceutics.* **2020**, *12*, 855.
(43) Rajput, R. L.; Narkhede, J. S.; Mujumdar, A.; Naik, J. B. Synthesis and Evaluation of Luliconazole Loaded Biodegradable Nanogels Prepared by PH-Responsive Poly (Acrylic Acid) Grafted Sodium Carboxymethyl Cellulose Using Amine Based Cross Linker for Topical Targeting: In Vitro and Ex Vivo Assessment. *Polym. Technol. Mater.* **2020**, *59* (15), 1654.
(44) Nasr, A. M.; Badawi, N. M.; Tartor, Y. H.; Sobhy, N. M.; Swidan, S. A. Development, Optimization, and In Vitro/In Vivo Evaluation of Azelaic Acid Transethosomal Gel for Antidermatophyte Activity. *Antibiotics* **2023**, *12* (4), 707.
(45) Bolla, P. K.; Meraz, C. A.; Rodriguez, V. A.; Deaguero, I.; Singh, M.; Yellepeddi, V. K.; Renukuntla, J. Clotrimazole Loaded Ufosomes for Topical Delivery: Formulation Development and in-Vitro Studies. *Molecules* **2019**, *24* (17), 3139.
(46) Ghose, A.; Nabi, B.; Rehman, S.; Md, S.; Alhakamy, N. A.; Ahmad, O. A. A.; Baboota, S.; Ali, J. Development and Evaluation of Polymeric Nanosponge Hydrogel for Terbinafine Hydrochloride: Statistical Optimization, in Vitro and in Vivo Studies. *Polymers (Basel).* **2020**, *12* (12), 2903.
(47) Araruna, M. K. A.; Brito, S. A.; Morais-Braga, M. F. B.; Santos, K. K. A.; Souza, T. M.; Leite, T. R.; Costa, J. G. M.; Coutinho, H. D. M. Evaluation of Antibiotic & Antibiotic Modifying Activity of Pilocarpine & Rutin. *Indian Journal of Medical Research.* **2012**, *135*, 252−254.
(48) Xie, Y.; Yang, W.; Tang, F.; Chen, X.; Ren, L. Antibacterial Activities of Flavonoids: Structure-Activity Relationship and Mechanism. *Curr. Med. Chem.* **2014**, *22* (1), 132.
(49) Ungureanu, C.; Pirvu, C.; Mindroiu, M.; Demetrescu, I. Antibacterial Polymeric Coating Based on Polypyrrole and Polyethylene Glycol on a New Alloy TiAlZr. *Prog. Org. Coatings* **2012**, *75* (4), 349.
(50) Akhtar, N.; Pathak, K. Preclinical and Clinical Aspects of Antimicrobial Drugs Delivered Through Ethosomal Vesicles. *Anti-Infective Agents* **2012**, *10* (1), 15.
(51) Moolakkadath, T.; Aqil, M.; Ahad, A.; Imam, S. S.; Iqbal, B.; Sultana, Y.; Mujeeb, M.; Iqbal, Z. Development of Transethosomes Formulation for Dermal Fisetin Delivery: Box−Behnken Design, Optimization, in Vitro Skin Penetration, Vesicles−Skin Interaction and Dermatokinetic Studies. *Artif. Cells Nanomed. Biotechnol.* **2018**, *46* (sup2), 755−765.
(52) Varshosaz, J.; Tabbakhian, M.; Mohammadi, M. Y. Formulation and Optimization of Solid Lipid Nanoparticles of Buspirone HCl for Enhancement of Its Oral Bioavailability. *J. Liposome Res.* **2010**, *20* (4), 286.
(53) Ali, A.; Aqil, M.; Imam, S. S.; Ahad, A.; Parveen, A.; Qadir, A.; Ali, M. H.; Akhtar, M. Formulation and Evaluation of Embelin Loaded Nanoliposomes: Optimization, in Vitro and Ex Vivo Evaluation. *J. Drug Delivery Sci. Technol.* **2022**, *72*, No. 103414.
(54) Jahan, S.; Aqil, M.; Ahad, A.; Imam, S. S.; Waheed, A.; Qadir, A.; Ali, A. Nanostructured Lipid Carrier for Transdermal Gliclazide Delivery: Development and Optimization by Box-Behnken Design. *Inorg. Nano-Metal Chem.* **2022**, 1.
(55) Delan, W. K.; Zakaria, M.; Elsaadany, B.; ElMeshad, A. N.; Mamdouh, W.; Fares, A. R. Formulation of Simvastatin Chitosan Nanoparticles for Controlled Delivery in Bone Regeneration: Optimization Using Box-Behnken Design, Stability and in Vivo Study. *Int. J. Pharm.* **2020**, *577*, 119038.
(56) Waheed, A.; Zameer, S.; Sultana, N.; Ali, A.; Aqil, M.; Sultana, Y.; Iqbal, Z. Engineering of QbD Driven and Ultrasonically Shaped Lyotropic Liquid Crystalline Nanoparticles for Apigenin in the Management of Skin Cancer. *Eur. J. Pharm. Biopharm.* **2022**, *180*, 269.
(57) Batool, S.; Zahid, F.; Ud-Din, F.; Naz, S. S.; Dar, M. J.; Khan, M. W.; Zeb, A.; Khan, G. M. Macrophage Targeting with the Novel Carbopol-Based Miltefosine-Loaded Transfersomal Gel for the Treatment of Cutaneous Leishmaniasis: In Vitro and in Vivo Analyses. *Drug Dev. Ind. Pharm.* **2021**, *47* (3), 440.
(58) Ali, A.; Ali, A.; Rahman, M. A.; Warsi, M. H.; Yusuf, M.; Alam, P. Development of Nanogel Loaded with Lidocaine for Wound-Healing: Illustration of Improved Drug Deposition and Skin Safety Analysis. *Gels* **2022**, *8* (8), 466.
(59) Tiwari, A.; Bag, P.; Sarkar, M.; Chawla, V.; Chawla, P. A. Formulation, Validation and Evaluation Studies on Metaxalone and Diclofenac Potassium Topical Gel. *Environ. Anal. Heal. Toxicol.* **2021**, *36* (1), e2021001.
(60) Rahman, M. S.; Al-Mahrouqi, A. I. Instrumental Texture Profile Analysis of Gelatin Gel Extracted from Grouper Skin and Commercial (Bovine and Porcine) Gelatin Gels. *Int. J. Food Sci. Nutr.* **2009**, *60* (SUPPL. 7), 229.
(61) Rarokar, N. R.; Menghani, S. S.; Kerzare, D. R.; Khedekar, P. B.; Bharne, A. P.; Alamri, A. S.; Alsanie, W. F.; Alhomrani, M.; Sreeharsha, N.; Asdaq, S. M. B. Preparation of Terbinafin-Encapsulated Solid Lipid Nanoparticles Containing Antifungal Carbopol® Hydrogel with Improved Efficacy: In Vitro, Ex Vivo and In Vivo Study. *Pharmaceutics* **2022**, *14* (7), 1393.
(62) El Atki, Y.; Aouam, I.; El Kamari, F.; Taroq, A.; Nayme, K.; Timinouni, M.; Lyoussi, B.; Abdellaoui, A. Antibacterial Activity of Cinnamon Essential Oils and Their Synergistic Potential with Antibiotics. *J. Adv. Pharm. Technol. Res.* **2019**, *10* (2), 63.
(63) Zafar, A.; Imam, S. S.; Yasir, M.; Alruwaili, N. K.; Alsaidan, O. A.; Warsi, M. H.; Ullah, S. N. M. N.; Alshehri, S.; Ghoneim, M. M. Preparation of NLCs-Based Topical Erythromycin Gel: In Vitro Characterization and Antibacterial Assessment. *Gels* **2022**, *8* (2), 116.
(64) Qizilbash, F. F.; Ashhar, M. U.; Zafar, A.; Qamar, Z.; Annu; Ali, J.; Baboota, S.; Ghoneim, M. M.; Alshehri, S.; Ali, A. Thymoquinone-Enriched Naringenin-Loaded Nanostructured Lipid Carrier for Brain Delivery via Nasal Route: In Vitro Prospect and In Vivo Therapeutic Efficacy for the Treatment of Depression. *Pharmaceutics* **2022**, *14* (3), 656.

https://doi.org/10.1021/acsomega.4c01718
ACS Omega 2024, 9, 27300−27311